Supporting Information for

Pt and Pt-Rh Supercrystals Self-assembled in N, N-Dimethylformamide

Lin-Xiu Dai,‡ Xin-Yu Wang,‡ Xiao-Yu Zheng and Ya-Wen Zhang*

Beijing National Laboratory for Molecular Sciences, State Key Laboratory of Rare Earth Materials Chemistry and Applications, PKU-HKU Joint Laboratory in Rare Earth Materials and Bioinorganic Chemistry, College of Chemistry and Molecular Engineering, Peking University, Beijing 100871, China.

Experimental details

Chemicals. $Pt(acac)_2$ (Pt wt. %>48.0%, Alfa Aesar Chemicals Co. Ltd, China), $RhCl_3 \cdot 3H_2O$ (A.R., Sinopharm Chemical Reagent Co. Ltd, China), N, N-dimethylformamide (DMF, A.R., Xilong Chemical Co. Ltd, China), ethanol (A.R.), acetone (A.R.).

Synthesis

Synthesis of Pt supercrystals. The precursors, 0.03 mmol of $Pt(acac)_2$ and 15 mL of DMF were put in a 25 mL Teflon-lined stainless steel autoclave and heated at 180 ℃ for 16 h. After the mixture was cooled, the black products were centrifuged by mixing 40 mL of acetone and washed by ethanol/acetone twice, and lastly dispersed in ethanol for the further characterizations.

Synthesis of Pt-Rh supercrystals. The synthesis of Pt-Rh supercrystals is similar to that of the Pt supercrystals except for the addition of 0.01 mmol $RhCl_3$.

Instrumentation. Transmission electron microscope (TEM), high-resolution transmission electron microscope (HRTEM), energy dispersive X-ray spectroscopy (EDS), were conducted on a FEG-TEM (JEM-2100F, JEOL, Japan) operated at 200 kV. The samples for TEM characterizations were prepared by dropping the colloid solution on copper grids coated with amorphous carbon and drying naturally. Small-angle X-ray diffraction (SAXRD) and wide-angle X-ray diffraction (WAXRD) analyses were performed on a Rigaku D/ MAX-2000 diffractometer (Japan). Fourier transform infrared (FTIR) spectra were recorded with a Bruker Tensor27 spectrophotometer and dry powders of the samples were examined using the KBr pressed pellet method. Dynamic light scattering measurements (DLS) were carried out using a spectrometer of standard design (ALV-5000/E/WIN Multiple Tau Digital Correlator) with a Spectra-Physics 2017 22 mW Ar laser (wavelength: 632.8 nm). X-ray photoelectron spectroscopy (XPS) analysis was taken on an Axi Ultra imaging photoelectron spectronmeter (Kratos, UK). Inductively coupled plasma-atomic spectroscopy (ICP-AES) analysis was performed on a Profile Spec ICP-AES spectrometer (Leeman, USA). The self-assembled structures were characterized by

scanning electron microscopy (SEM, Hitachi S4800, 10 kV).

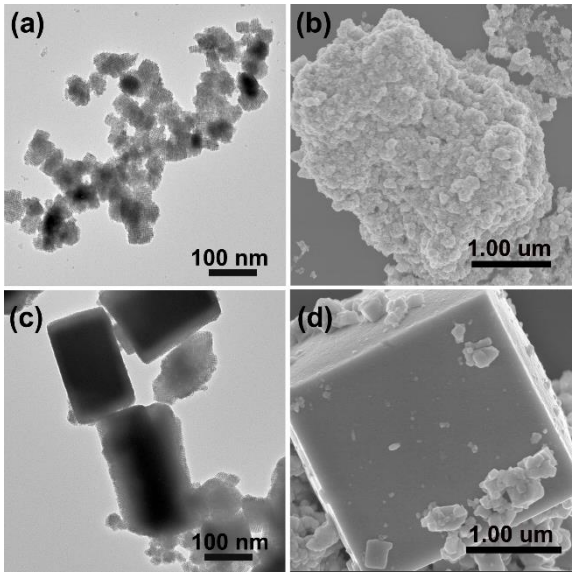

Figure S1. TEM (a) and SEM images (b) of Pt supercrystals. TEM (c) and SEM images (d) of Pt-Rh supercrystals.

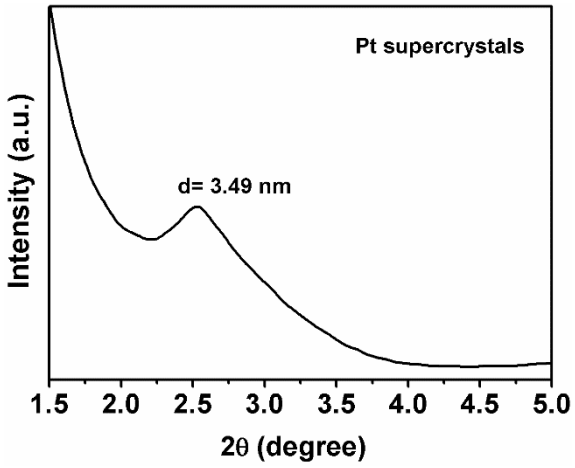

Figure S2. Small-angle XRD pattern of Pt supercrystals.

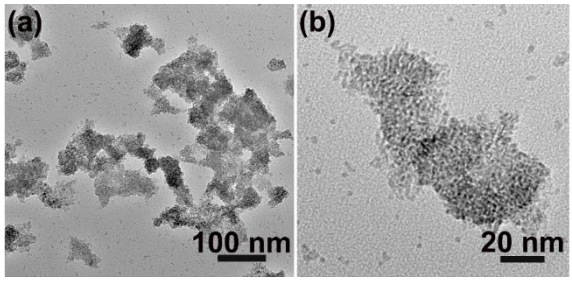

Figure S3. TEM images of Rh nanoparticulate assemblies.

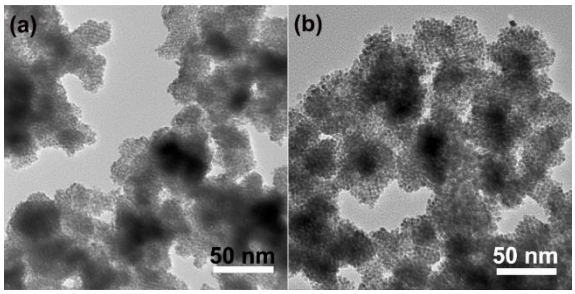

Figure S4. (a) TEM image of Pt-Pd supercrystals with using $PdCl_2$ as the metal precursor, and (b) TEM image of Pt-Ni supercrystals with using $NiCl_2$ as the metal precursor, under the same reaction conditions as that of Pt-Rh supercrystals.

Computational Details.

All DFT calculations were performed with the Vienna ab initio simulation package (VASP). Kohn−Sham equations were expanded into plain waves. (Ref. S1-S3) The exchange-correlation energy functional was described in the Perdew−Burke−Ernzerh of generalized gradient approximation (GGA-PBE). (Ref. S4) In the Brillouin zone, the 5 × 5 × 1 Monkhorst−Pack special k-point mesh was automatically generated. The atoms were presented by projector augmented-wave (PAW) pseudopotentials. (Ref. S5) The kinetics energy cutoff for the plane-wave basis set was 400 eV.

For surface adsorption calculations, (100) and (111) surface exposed 3 × 3 × 6 metal supercells with three fixed layers and 15 Å of vacuum was built for the simulation. The structure of the DMF adsorbates and the Pt atoms in the top three layers were allowed to relax to their lowest energy configuration. Each structure was relaxed until the residual force was less than 0.02 eV/Å.

The adsorption energy E_{ads} is defined by the following equation: $E_{ads} = E_{Pt/DMF} - E_{Pt} - E_{DMF}$, in which $E_{Pt/DMF}$ is the total energy of the slab with adsorbates DMF, E_{Pt} is the energy of the Pt slab, and E_{DMF} is the energy of the DMF adsorbates in gas phase (15 Å ×15 Å ×15 Å).

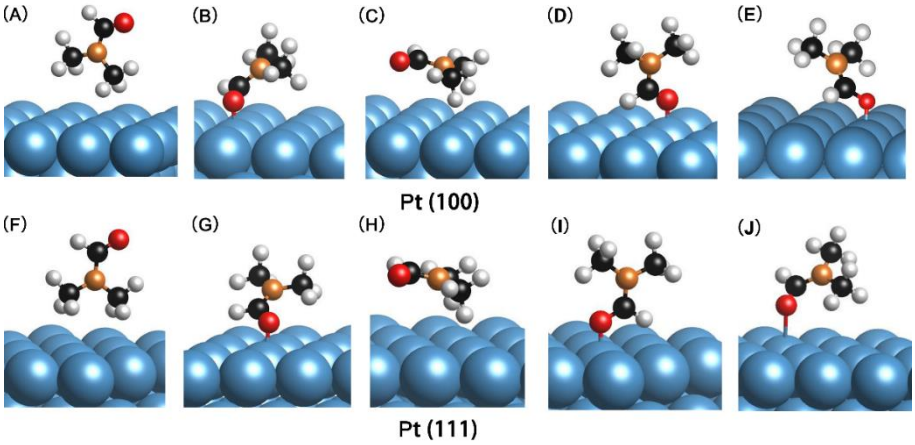

Figure S5. Possible calculated adsorption configurations of the DMF molecule on 3×3×3 Pt (100) and Pt (111) slabs.

For Pt (100) surface, D means the most stable adsorption configuration of the DMF against Pt surface with oxygen adsorbed on Pt-atop position. Other four possible calculated configurations (A, B, C and E) have higher adsorption energies than D. Similarly, for Pt (111) surface, G represents the most stable configuration of all. Other configurations listed (F, H, I, and J) have higher adsorption energies than G. Hence D and G were the most stable configurations over the Pt (111)-DMF and Pt (100)-DMF adsorption system, respectively. Furthermore, we used Pt (3×3×6) slabs with 3 top layers relaxed to compare the adsorption energies of two configurations. The adsorption energies were mentioned in the main text. For D in the Pt (100)-DMF system, the calculated length of C-O bond is 1.26 Å, which is slightly longer than that of C-O bond in the DMF molecule with 1.23 Å. The calculated length of Pt-O bond is 2.15 Å, suggesting the possibility of oxygen coordinating with Pt, which may stretch the C-O bond.

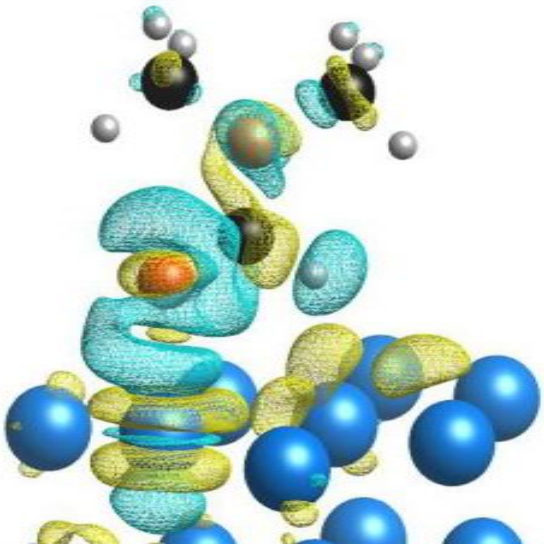

Figure S6. Charge density difference of DMF adsorbed on Pt (100) surface. The blue, red, orange, black, grey balls represent Pt, O, N, C, H atoms, respectively. The non-spherical clouds represent the charge density difference. Yellow clouds mean the positive charge density difference, green clouds mean the negative values.

Then we did Bader analysis about the system and calculated the charge density difference. For the DMF molecule adsorbed on Pt (100) surface, the partial charge of each atom was compared using the Bader Analysis Method, which indicated a charge transfer of 0.07 e- from DMF to Pt layers. For further evaluation of the interactions between DMF and metal surface, charge density difference Δρ ($\Delta\rho=\rho_{Pt\text{-}DMF}-\rho_{Pt}-\rho_{DMF}$, $\rho_{Pt\text{-}DMF}$, ρ_{Pt} and ρ_{DMF} represent the charge density of the DMF-Pt system, metal slab and adsorbate molecule, respectively.) was calculated and plotted in visually 3D image. (Ref. S6)

A loss of charge density between the three atoms along the C-O-Pt axis, corresponding to the repulsive σ-interaction between Pt-O and C-O bonds, is observed from charge density difference plots in Fig. S4. While the charge increasing in the perpendicular direction can be attributed to the π interaction. (Ref. S7) We can also

find that the charge density increases around the neighbor Pt atoms uncoordinating with DMF molecules. The interactions between Pt atoms and DMF molecules indicate that the d-orbitals of the Pt atoms on the top-layer may bond with the π-orbitals of C-O. The polarization of charge away from the coordinated Pt atom to the surrounding metal and d-d rehybridization on the Pt atoms can decreases the d-σ character and increases the d-π interaction. (Ref. S8) This could be significant for the π-bonding.

Hence, the weak adsorption energy calculated (only -0.5 eV) results from a balance of σ-binding repulsion and π-orbitals bonding. (Ref. S9) Meanwhile, the π-d attraction of DMF molecules and Pt atoms delocalizes the electrons of the adsorption system and thus weakens the C-O bond, which is supported by the weaker vibrating peak at 1640 cm^{-1} compared with that of pure DMF (1680 cm^{-1}) in the FTIR results of Pt supercrystals (Fig. S7).

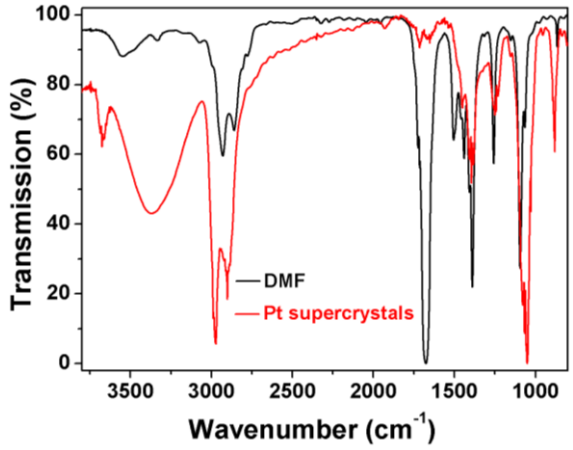

Figure S7. FTIR spectrum of the as-obtained Pt supercrystals with pure DMF as a reference.

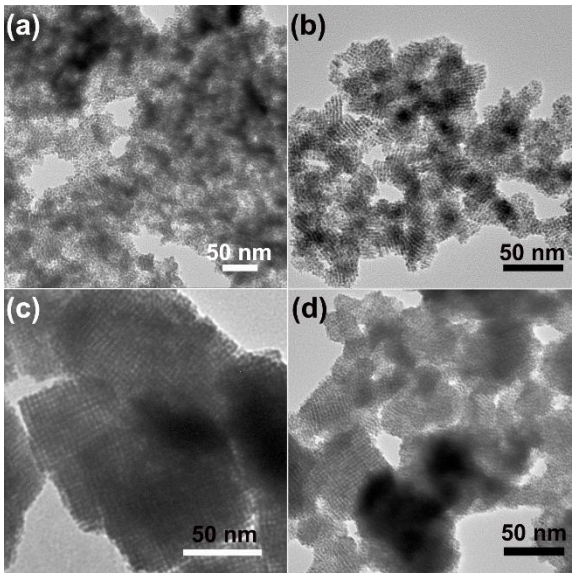

Figure S8. Pt supercrystals obtained at different reaction temperature: (a) 140 °C, (b) 160 °C, (c) 180 °C, (d) 200 °C.

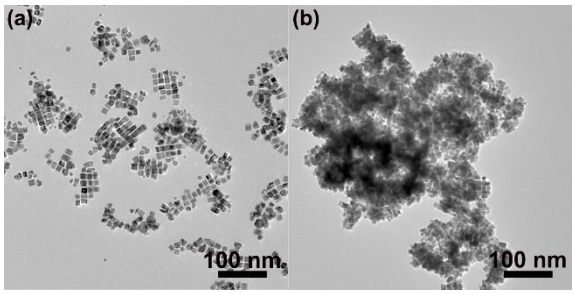

Figure S9. (a) TEM image of monodispersed Pt nanocubes, and (b) TEM image of post-assembled Pt supercrystals using the former nanocubes as the building blocks.

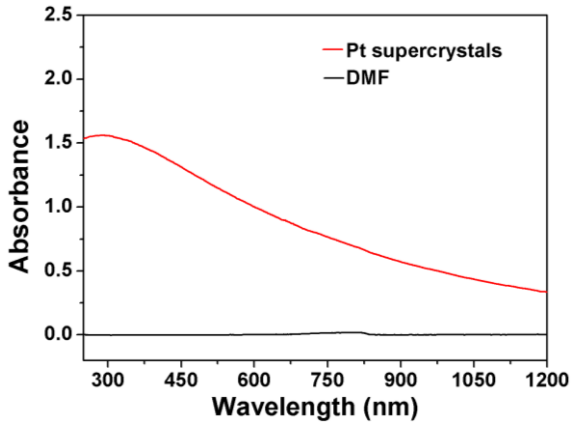

Figure S10. UV-*vis* spectra of Pt supercrystals and DMF dispersed in ethanol.

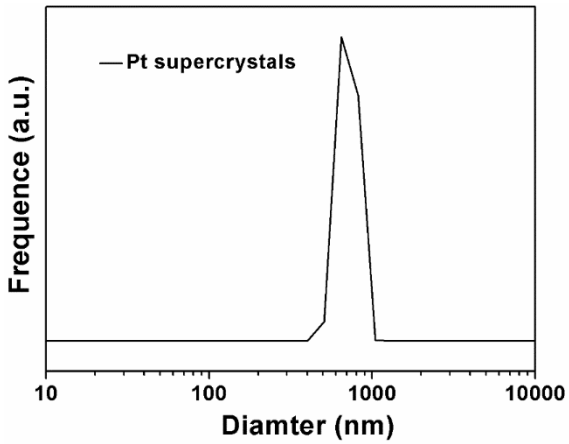

Figure S11. DLS curve of the size distribution of the as-prepared Pt supercrystals in DMF.

Ref. S1 G. Kresse, J. Hafner, *Phys. Rev. B*, 1993, **47**, 558.
Ref. S2 G. Kresse, J. Hafner, *Phys. Rev. B*, 1993, **48**, 13115.
Ref. S3 G. Kresse, J. Hafner, *Phys. Rev. B*, 1993, **49**, 14251.
Ref. S4 J. P. Perdew, K. Burke, M. Ernzerhof, *Phys. Rev. Lett.*, 1996, **77**, 3865.
Ref. S5 P. Blochl, *Phys. Rev. B*, 1994, **50**, 17953.
Ref. S6 K. Momma, F. Izumi, *J. Appl. Crystallogr.*, 2011, **44**, 1272.

Ref. S7 A. Nilsson, L. G. M. Pettersson, *Surf. Sci. Reps*, 2004, **55**, 49.
Ref. S8 P. Bennich, T. Wiell, O. Karis, M. Weinelt, N. Wassdahl, A. Nilsson, M. Nyberg, L. G. M. Pettersson, J. Stohr, M. Samant, *Phys. Rev. B*, 1998, **57**, 9274.
Ref. S9 A. Nilsson, L. G. M. Pettersson, J. K. Norskov, *Chemical Bonding at Surfaces and Interfaces*, Elsevier, **2008**.